Modern Research in Catalysis, 2015, 4, 97-106
Published Online October 2015 in SciRes. http://www.scirp.org/journal/mrc
http://dx.doi.org/10.4236/mrc.2015.44012

Catalytic Performance of $La_{0.6}Ca_{0.4}Fe_{1-x}Ni_xO_3$ Perovskites in DME Oxidation

Gina Pecchi[1*], Ruddy Morales[1], Daniela Salinas[1], Eduardo J. Delgado[1], José Luis García Fierro[2]

[1]Facultad Ciencias Químicas, Universidad de Concepción, Concepción, Chile
[2]Instituo Catálisisy Petroleoquímica, CSIC, Cantoblanco, Madrid, Spain
Email: *gpecchi@udec.cl

Received 14 August 2015; accepted 13 October 2015; published 16 October 2015

Copyright © 2015 by authors and Scientific Research Publishing Inc.
This work is licensed under the Creative Commons Attribution International License (CC BY).
http://creativecommons.org/licenses/by/4.0/
Open Access

Abstract

Substituted $La_{0.6}Ca_{0.4}Fe_{1-x}Ni_xO_3$ ($0.0 \le x \le 1.0$) perovskite-type oxides prepared by the amorphous citrate method have been investigated as catalysts in the dimethyl ether (DME) oxidation reaction. The samples with an $x \le 0.3$ composition show an orthorhombic structure, while the intermediate compositions with $0.5 \le x \le 0.9$ show a less crystalline orthorhombic perovskite structure with segregated phases that increase upon increasing the Ni content. The progressive substitution of Fe^{3+} by Ni^{2+} in $La_{0.6}Ca_{0.4}FeO_3$ entails the progressive formation of oxygen vacancies and Fe^{4+} species for Ni substitution degrees of $x \le 0.5$. For larger degrees of substitution with $x > 0.7$, segregated phases and a progressive loss of the perovskite structure are detected. The highest catalytic performance for the total combustion of DME is obtained from equimolar substitution in the B-site position ($Fe_{0.5}Ni_{0.5}$), in which a large extent of Fe^{4+} species and oxygen vacancies are present.

Keywords

DME, Perovskites, Oxidation, Iron, Nickel

1. Introduction

Simple perovskites with a basic formula of ABO_3 have been consistently proposed since the 1970s [1] as alternative catalysts for the deep oxidation of hydrocarbons due to their lower cost in comparison with their noble metal counterparts [2]. The perovskite lattice tolerates wide variations in the nature of the A and B cations and allows a large number of substitutions involving one or both of the cations [3] [4]. Pure and substituted lanthanide perovskites with A = La and B = a first row transition element have received a great amount of attention as

*Corresponding author.

How to cite this paper: Pecchi, G., Morales, R., Salinas, D., Delgado, E.J. and Fierro, J.L.G. (2015) Catalytic Performance of $La_{0.6}Ca_{0.4}Fe_{1-x}Ni_xO_3$ Perovskites in DME Oxidation. *Modern Research in Catalysis*, **4**, 97-106.
http://dx.doi.org/10.4236/mrc.2015.44012

oxidation catalysts. It is well established that the nature and extent of the metal substituted in position A may also stabilize an unusual oxidation state of the cation in position B and/or produce oxygen vacancies [5]-[7]. In $LaFeO_3$, the substitution of the trivalent A-site metal ion with a bivalent metal cation (A') modifies the oxidation state of the B-site metal cation by the formation of structural defects, leading to non-stoichiometric ratios and thus modifying the catalytic activity. Pecchi *et al*. [8] [9] have reported an increase in the oxygen mobility, reducibility and catalytic reaction rate in partially A-cation substituted $LaFeO_3$. Conversely, the partial substitution of cation B by B' also improves the perovskite stability or enhances its redox efficiency [10] [11]. A significant enhancement in the catalytic activity in oxidation reactions of $LaFeO_3$ with a B cation partially substituted with Ni [12] and Zn [13] has also been reported. Noticeable increases in the oxidation reaction rate have also been reported for a double substitution in the A- and B-site positions of pure lanthanum manganite with 10% of Co and Ag, respectively [10]. Among the oxidation reactions, dimethyl ether combustion (DME) has been recently studied on Ce-doped manganese oxide octahedral molecular sieves (OMS-2) [14], cryptomelane oxides [15] and layered pillared Al_2O_3 [16] as an alternative low-cost replacement for liquefied petroleum gas (LPG) and diesel fuel due to its easy transportation, lower emission of polluting particles and higher thermal efficiency. The widely accepted mechanism for catalytic combustion on perovskite-type oxides at lower temperature (<400˚C) is closely related to the interaction of surface oxygen with the reactants. It was proposed that to improve the activity and enhance the redox efficiency of $La_{0.6}Ca_{0.4}FeO_3$, a family of substituted $La_{0.6}Ca_{0.4}Fe_{1-x}Ni_xO_3$, $0 \le x \le 1.0$, perovskites were synthesized and their surface, structural and catalytic properties were characterized. Based on this evidence, the synthesis, characterization and effect of the substitution in $La_{0.6}Ca_{0.4}Fe_{1-x}Ni_xO_3$ (x = 0.0, 0.1, 0.3, 0.5, 0.7, 0.9, 1.0) perovskites calcined at 700˚C on the catalytic activity of DME combustion are addressed.

2. Experimental

2.1. Preparation

Substituted $La_{0.6}Ca_{0.4}Fe_{1-x}Ni_xO_3$ ($0.0 \le x \le 1.0$) perovskites were prepared by adding stoichiometric amounts of an aqueous solution of the metal nitrates to an aqueous solution of citric acid with a 10% of excess above the number of cations. The resulting solution was stirred for 15 min at room temperature and slowly evaporated at 70˚C under vacuum in a rotary evaporator until gel formation was reached. Then, the gel was dried in an oven, with a slow increase in the temperature up to 250˚C where it was maintained overnight in order to obtain a solid amorphous citrate precursor. The resulting powder was crushed and sieved to obtain the required particle size (<200 μm), and then, it was calcined at 700˚C in air for 10 h.

2.2. Characterization

Chemical analysis of the samples was performed by atomic absorption spectrometry (AAS) using a Perkin Elmer model 3100 instrument. The specific areas were calculated using the BET method from the nitrogen adsorption isotherms, which were recorded at the liquid nitrogen temperature on a Model ASAP 2010 Micromeritics apparatus. The amount of tetravalent iron contained in the calcined samples was determined by a redox titration according to the equation $Fe^{4+} + Fe^{2+} = 2Fe^{3+}$ [17] [18] by dissolving, in an acid medium, the samples in a known excess of a Mohr salt standard solution and titrating the excess of Fe(II) with $K_2Cr_2O_7$. The titration was performed twice for each sample with the reproducibility of the results always within 2%. X-ray powder diffraction (XRD) patterns were obtained with nickel-filtered CuKα_1 radiation (λ = 1.5418 Å) using a Rigaku diffractometer and were collected in a 2θ range of 20˚ to 70˚. TPR and oxygen TPD experiments were performed in a TPR/TPD 2900 Micromeritics system with a thermal conductivity detector. Samples of approximately 20 mg were placed in a U-shaped quartz tube, purged in a synthetic air stream for 1 h at 500˚C and then cooled to ambient temperature. The reduction profiles were recorded by passing 5% H_2/Ar from ambient temperature to 700˚C. For the TPD experiments, the samples were preheated in an O_2 flow for 1 h at 700˚C and then cooled to room temperature in the same atmosphere. After switching the atmosphere to a helium flow, the oxygen desorption was monitored using a TCD. Surface analysis was performed on a VG Escalab 200R electron spectrometer equipped with an Mg Kα X-ray source and a hemispherical electron analyzer. Prior to analysis, all of the samples were degassed at 300˚C for 1 h inside the pre-treatment chamber of the spectrometer. The charging effects on the samples were corrected by taking the C1s peak of adventitious carbon at 284.9 eV.

2.3. Catalytic Activity

The evaluation of the catalytic activity in the total DME oxidation was performed in a conventional flow reactor

at atmospheric pressure using 0.3 g of the catalyst powder (40 - 60 mesh) diluted with 1.5 g of CSi. Prior to the catalytic tests, the samples were pretreated under a purge of the mixed gas at 120˚C for 30 min to stabilize the system. Then, the temperature was linearly increased up to the required temperature, maintained at that temperature for 20 min and raised to a new temperature using the same heating rate (1˚C·min^{-1}). Several isothermal steps were performed until complete conversion. The reactant mixture was fed into the reactor to maintain a gas hourly space velocity (GHSV) of 10 dm^3·g^{-1}·h^{-1}, [15] and a reaction mixture of DME:O_2:He (molar ratio) of 1:10:89 was used. Effluents of the reactor were analyzed using a Hewlett Packard HP 4890D on-line gas chromatograph with a thermal conductivity detector. Helium was used as the carrier gas, and the column used was a 30-m Supelco 25,462 capillary. A Shimadzu GCMS-QP5050 quadrupole mass spectrometer was used to detect small traces of products.

3. Results and Discussion

3.1. Chemical Composition and Texture

The elemental compositions of the $La_{0.6}Ca_{0.4}Fe_{1-x}Ni_xO_3$ perovskites determined by AAS show Fe and Ni contents similar to the nominal ones, as it can be seen in **Table 1**. The La and Ca contents (not shown) are much closer to the nominal contents of 40.5% and 7.4%, respectively. The specific BET areas, also summarized in **Table 1**, do not show large differences that are dependent upon the Ni or Fe content, although they are lower for the doubly substituted perovskites [19] [20].

3.2. Structural Analysis

X-ray diffraction patterns of the $La_{0.6}Ca_{0.4}Fe_{1-x}Ni_xO_3$ oxides after calcination at 700˚C are displayed in **Figure 1(a)**. For the non B-site substituted solids ($La_{0.6}Ca_{0.4}FeO_3$ and $La_{0.6}Ca_{0.4}NiO_3$), the sharp reflections located at the expected 2θ values confirm that Ca^{2+} has been built-into the perovskite lattice for only $La_{0.6}Ca_{0.4}FeO_3$, [8] due to that for $La_{0.6}Ca_{0.4}NiO_3$, no perovskite structure is detected. For the A- and B-site substituted solids, two different structural behaviors are observed for lower ($x \leq 0.3$) and higher ($x \geq 0.5$) degrees of Ni-substitution. For x = 0.0, 0.1, and 0.3, isostructural perovskites corresponding to orthorhombic $LaFeO_3$ (37 - 1493) are formed with no segregated phases of O_3, thus supporting the hypothesis that small amounts of iron can be substituted by nickel cations [9]. **Figure 1(b)** shows a close up of the diffraction peaks at $2\theta = 57^\circ$. The shift towards higher 2θ values is indicative of a smaller interplanar distance or a decrease in the cell volume, which cannot be attributed to lanthanum or calcium due to their constant compositions. Therefore, the decreases in the cell volume can be achieved by the stabilization of metal ions in a high oxidation state in the perovskite structure. Doping with Ni^{2+} into the lattice of the perovskite structure induces the partial oxidation of the B-site cation ($Fe^{3+} \rightarrow Fe^{4+}$) [21]. The differences in the ionic radii of Fe^{4+} (0.0585 nm) and Fe^{3+} (0.0645 nm) explain the corresponding shift in **Figure 1(b)**, which is in agreement with previous results reported for other iron-based perovskites [12] [18]. For a higher Ni content, $0.5 \leq x \leq 0.9$, the most intense diffraction peak of the perovskite structure appears at a higher 2θ value (58˚), indicative of the formation of a less crystalline orthorhombic $LaNiO_3$ (34 - 1028) perovskite structure with a number of segregated phases, which were identified as CaO (28 - 0775), La_2NiO_4 (11 - 557) and NiO (22 - 1189). These results indicate that iron ions remain incorporated within an orthorhombic perovskite structure only for $x \leq 0.3$. For larger Ni contents, a large amount of segregated phases as well as the formation of a less crystalline perovskite structure are obtained.

3.3. Surface Structure

The XPS experiments of O1s, $Ca2p_{3/2}$, $Fe2p_{3/2}$ and $Ni2p_{1/2}$ spectra for a representative sample are shown in **Figure 2**. The broad peak for $Ca2p_{3/2}$ can be deconvoluted into two peaks and the O1s into three peaks. The three components obtained from the fitting of the O1s peak can be assigned to the following: 1) surface lattice oxygen species (O_{latt}^{2-}) at 529.2 eV; 2) weakly adsorbed oxygen species (O_{2ads}^{2-} or O_{ads}^{-}) at 531.0 eV arising from lattice [La-O-M] bonds; and 3) loosely adsorbed super peroxide species (O_{2ads}^{-}) such as hydroxyl and/or carbonate groups at 532.3 eV [22]-[24]. **Table 2** summarizes the BEs of $La3d_{5/2}$, $Fe2p_{3/2}$ and $Ni2p_{1/2}$ core-levels as well as the extent (%) of the contribution of each peak for the $Ca2p_{3/2}$ and O1s. As expected for La-containing perovskites, the BE of C1s at 289.8 eV, which is not included in the Table, does not change and corresponds to the presence of surface carbonates [25]. The BE of the most intense peaks of doublets for $La3d_{5/2}$ at 834.8 eV and

$Fe2p_{3/2}$ at 710.3 eV as well as the least intense peak for $Ni2p_{1/2}$ at 873.4 were almost constant even though the satellite line placed at ca. 881.2 eV is indicative of the presence of Ni^{2+} ions on the surface. It must be emphasized that the higher BE contribution of the $La3d_{3/2}$ peak overlaps with the $Ni2p_{3/2}$ peak. This overlapping may mask not only the accurate measurement of the BE of nickel but also its intensity. To overcome this complication, the $Ni2p_{1/2}$ was measured. The surface $Ca2p_{3/2}$ at 346.8 eV, identified with a larger oxidized calcium content, increases upon increasing Ni contents, which is indicative of a larger extent of surface highly dispersed cal-

Table 1. Fe and Ni bulk composition (nominal values in parentheses) in wt.%, specific area, extent of Fe^{4+} (%) and total desorbed oxygen.

	Fe[1]	Ni[1]	S_{BET}, $m^2 \cdot g^{-1}$	Fe^{4+},%	oxygen $\mu mol \cdot g^{-1}$
$La_{0.6}Ca_{0.4}FeO_3$	26.4 (27.5)	---	28	3.7	314
$La_{0.6}Ca_{0.4}Fe_{0.9}Ni_{0.1}O_3$	25.8 (24.7)	3.0 (2.9)	24	8.3	377
$La_{0.6}Ca_{0.4}Fe_{0.7}Ni_{0.3}O_3$	19.9 (19.1)	8.9 (8.7)	23	15.2	566
$La_{0.6}Ca_{0.4}Fe_{0.5}Ni_{0.5}O_3$	13.1 (13.6)	13.7 (14.3)	27	13.6	912
$La_{0.6}Ca_{0.4}Fe_{0.3}Ni_{0.7}O_3$	7.9 (8.2)	20.9 (20.0)	23	9.0	701
$La_{0.6}Ca_{0.4}Fe_{0.1}Ni_{0.9}O_3$	2.8 (2.7)	27.3 (25.6)	22	3.2	631
$La_{0.6}Ca_{0.4}NiO_3$	---	29.7 (28.5)	29	--	625

[1]Estimated error below 5%

Table 2. BE (eV) of core-levels of $La3d_{5/2}$, $Fe2p_{3/2}$ and $Ni2p_{1/2}$ as well as the extent (%) of $Ca2p_{3/2}$ and O1s.

	La $3d_{5/2}$	Fe $2p_{3/2}$	Ni $2p_{1/2}$	Ca $2p_{3/2}$		O 1s, %		
				346.2	346.8	528.9	530.9	532.5
$La_{0.6}Ca_{0.4}FeO_3$	833.9	710.1	---	83	17	44	39	17
$La_{0.6}Ca_{0.4}Fe_{0.9}Ni_{0.1}O_3$	834.6	710.6	873.3	64	36	46	37	17
$La_{0.6}Ca_{0.4}Fe_{0.7}Ni_{0.3}O_3$	834.7	710.5	873.4	60	40	45	35	20
$La_{0.6}Ca_{0.4}Fe_{0.5}Ni_{0.5}O_3$	834.6	710.5	873.4	36	64	28	44	28
$La_{0.6}Ca_{0.4}Fe_{0.3}Ni_{0.7}O_3$	834.8	710.7	873.3	41	59	33	42	25
$La_{0.6}Ca_{0.4}Fe_{0.1}Ni_{0.9}O_3$	834.5	710.4	873.2	36	64	29	40	31
$La_{0.6}Ca_{0.4}NiO_3$	834.8	---	873.1	38	62	28	36	36

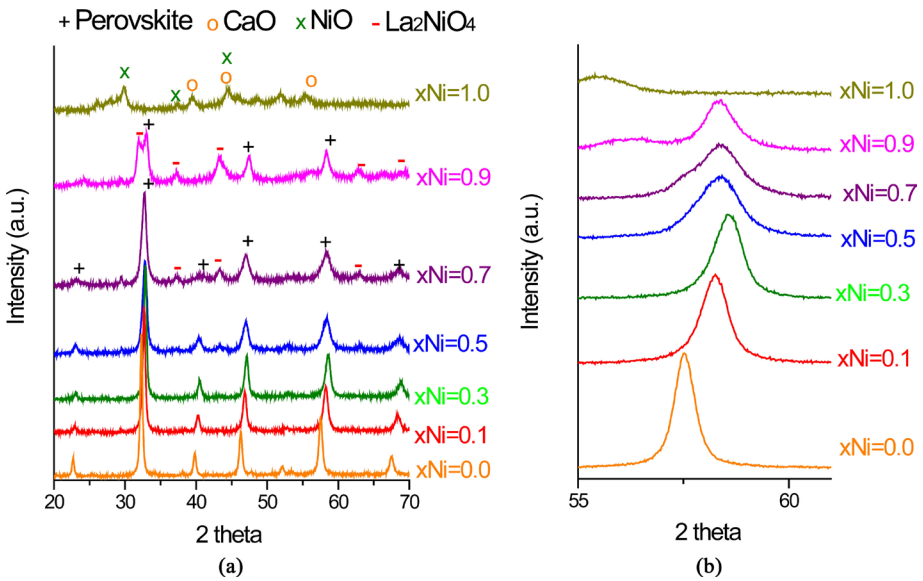

Figure 1. X-ray diffraction patterns for various 2θ values: (a) 20˚ - 70˚; (b) 55˚ - 65˚.

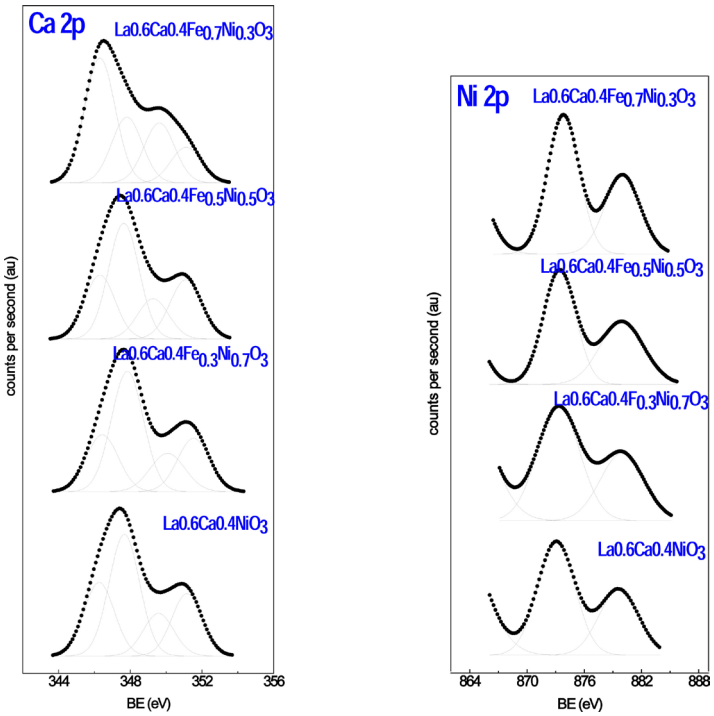

Figure 2. Ca2p, O1s, Ni2p, Fe2p core-level spectra for representative solids.

cium oxides [26]. The changes in the extent of the stronger electrophilic weakly adsorbed oxygen species (O_{2ads}^{2-} and O_{ads}^{-}) at BEs lower than 530.9 eV could be related to electronic changes [27] [28] in the perovskite structure, and the O1s species higher than 531 eV could be related to the thermal treatment before the XPS experiment. The surface atomic ratios for Ni/La + Ca, Ca/La + Ca and Fe/La + Ca calculated using atomic sensitivity factors for the Mg Kα source [22] are displayed in **Figure 3**. For comparison, the bulk ratios were also incorporated. It can be seen that the Ni/La + Ca surface ratio is always higher compared to the nominal ones, which is indicative of Ni-enrichment related to the increase of NiO and La_2NiO_4 segregated phases. The Ca/La + Ca surface ratio is slightly higher than that from the nominal compositions and did not show significant differences that were dependent upon the Ni content. For the surface Fe/La + Ca ratio, two different trends can be seen. The ratio is lower than the nominal one for lower degrees of Ni substitution ($x \leq 0.3$) and the same value as the nominal one for higher Ni contents ($x \geq 0.5$). This result indicates a surface Ni-enrichment in the total studied extent of Ni, which is indicative that separate Ni-La(Ca)-O species are developed throughout the entire compositional range with no segregation of iron species.

3.4. Redox Properties

To gain insight into the changes in the oxidation state of the B-cations, redox titrations and O_2-TPD profiles were carried out. In **Table 1**, the extent of Fe^{4+}, calculated from redox titrations, shows larger values for $x = 0.3$ and 0.5. Due to the increases in the Ni content, which decrease the Fe extent, the normalized atomic (Fe^{4+}/total Fe) ratio based upon the Ni content is shown in **Figure 4**. Again, the progressive increase of the Fe^{4+}/Fe total ratio is a measurement of the progressive insertion of Ni^{2+} into the perovskite structure up to $x = 0.5$. The larger extent of segregated phases for higher Ni contents ($x > 0.7$) and the smaller total Fe content increases both the Fe^{4+}/total Fe ratio and the uncertainly of the value, and these measurements do not help to obtain clear conclusions. In the O_2-TPD profiles shown in **Figure 5**, the expected physisorption occurred at approximately 90˚C, and two chemisorbed oxygen species between 200˚C and 600˚C [29] are observed. The lower temperatures (T < 300˚C) correspond to weakly chemisorbed oxygen on oxygen vacancies [30], and the highest temperatures (300˚C < T < 600˚C) correspond to oxygen species from boundaries or defects [31] called surficial oxygens [32]. For lower Ni contents ($x \leq 0.3$), only a broad desorption peak at 300˚C with a shoulder at 240˚C is observed, whereas for higher Ni contents ($x \geq 0.5$), a new and well-defined oxygen desorption peak at 340˚C, with no shift

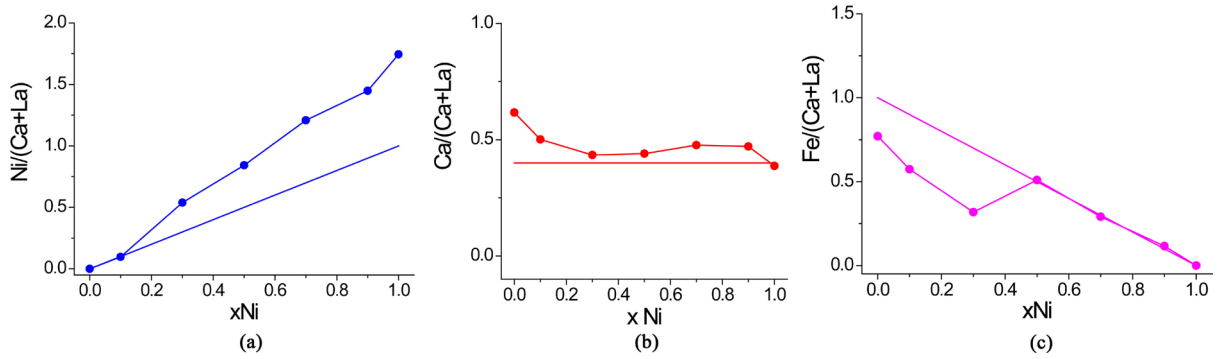

Figure 3. Surface ratios: (●) Ni/Ca + La, (Δ) Ca/Ca + La, and (▲) Fe/Ca + La. (-) bulk ratio.

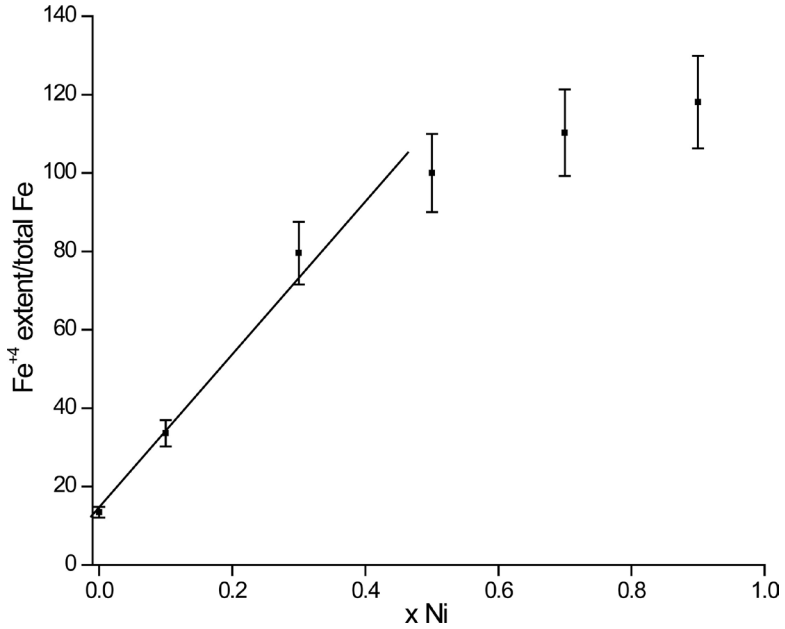

Figure 4. Fe^{4+}/Fe total versus the Ni content.

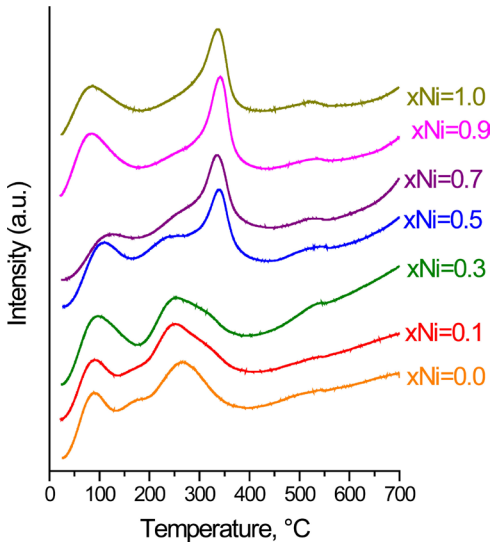

Figure 5. Oxygen desorption profiles.

dependent upon the Ni content, indicates the appearance of a large extent of new chemisorbed oxygen species. These new chemisorbed oxygens for higher degrees of Ni substitution ($x \geq 0.5$) can be associated with the large extent of segregated phases [31] in line with the XPS and XRD results. Because TPD-MS experiments confirm that the evolved gas and He flow only contain oxygen, the deconvolution of the oxygen desorption curves using a Lorentzian peak shape allow the calculation of the amount of desorbed oxygen. The total chemisorbed oxygen species between 200˚C and 600˚C based upon the Ni content shown in **Table 1** indicate formation of oxygen vacancies achieved, at lower substitution levels of $x \leq 0.5$ fundamentally by the oxidation of a portion of the iron ions from Fe^{3+} to Fe^{4+}. At higher Ni doping levels the oxygen vacancies can be related to the large extent of surface segregated phases. The maximum is reached for the $x = 0.5$ perovskite. The TPR profiles under a H_2/Ar flow up to 700˚C are shown in **Figure 6**. The $0.1 \leq x \leq 0.9$ solids show an intermediate behavior between the lowest $La_{0.6}Ca_{0.4}FeO_3$ and the largest $La_{0.6}Ce_{0.4}NiO_3$ reducible solids. The reduction profile for $La_{0.6}Ca_{0.4}FeO_3$ shows a single reduction peak at approximately 260˚C, which can be attributed to the reduction of Fe^{4+} to Fe^{3+} [9], which increases in the solids up to $x \leq 0.7$. The shift towards lower temperatures indicates an increase in and the easier reducibility of Fe^{4+} as a consequence of the presence of Ni^{2+} in the perovskite lattice [18] [20] [33]. For the higher Ni substituted perovskites ($x \geq 0.5$) the TPR profiles do not show such a clear trend.

3.5. Catalytic Activity

The catalytic activity for DME combustion under an excess of oxygen was measured as a function of the temperature up to complete combustion. Water and CO_2 were the only observed products. The typical experimental sigmoidal curves displayed in **Figure 7** indicate that the reaction starts at 170˚C until complete conversion at 300˚C. To quantify the catalytic behavior, in **Table 3** the ignition temperatures (T_i^{50}), defined as the temperatures to achieve 50% of reactant conversion, and the reaction rate at a low conversion level (<10%) evaluated at 195˚C are compiled. The larger catalytic activity, *i.e.*, the lowest ignition temperature and larger reaction rate, is shown by the equimolar $La_{0.6}Ca_{0.4}Fe_{0.5}Ni_{0.5}O_3$ perovskite. A decrease in the reaction rate and a parallel increase in the ignition temperature for both the lower $x \leq 0.3$ and higher $x \geq 0.7$ values are also detected. It has been noted that structural defects and oxygen mobility are the most important factors controlling the catalytic activity of perovskites in oxidation reactions [34]. Moreover, the catalytic activity for the combustion reaction has been found to be closely related to the activation of gaseous oxygen species and chemisorbed oxygen species [30] [35] as well as the redox properties of Fe^{4+} species [8]. Therefore, the fairly good correlation between the reaction rate and chemisorbed oxygens shown in **Figure 8** supports the importance of desorbed oxygen in the studied systems. Due to that the Fe content is not constant in the studied samples; it has not been possible to search for a correlation between the reaction rate and the extent of Fe^{4+}.

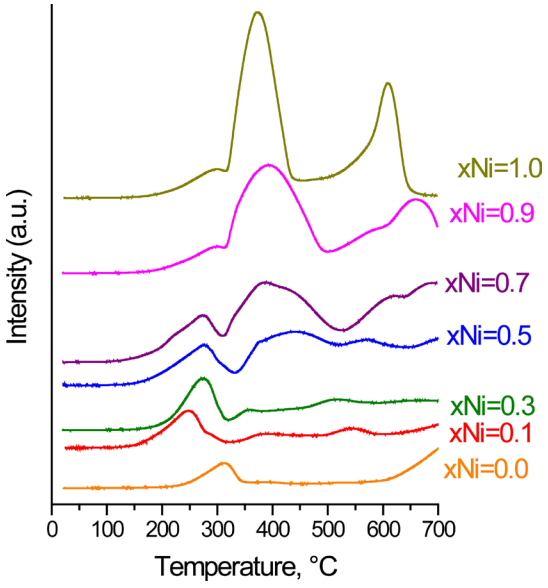

Figure 6. Temperature-programmed reduction (TPR) profiles.

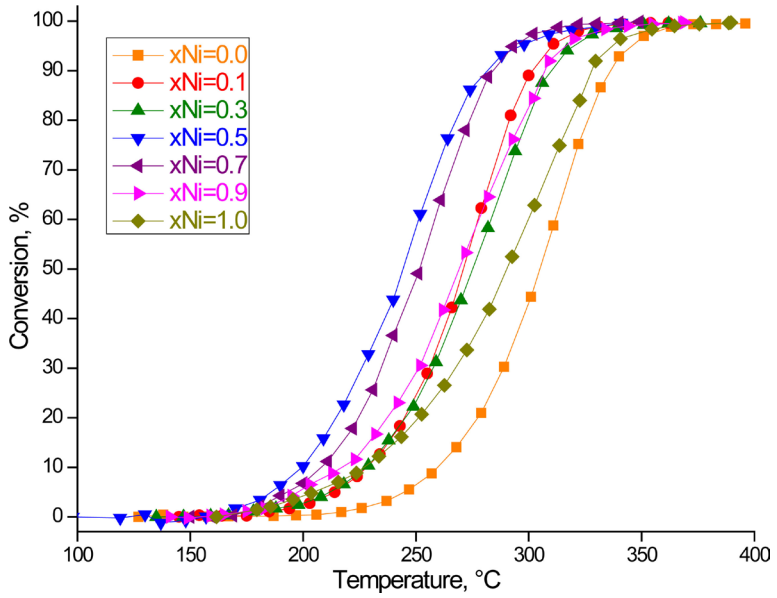

Figure 7. Stationary state conversion plots.

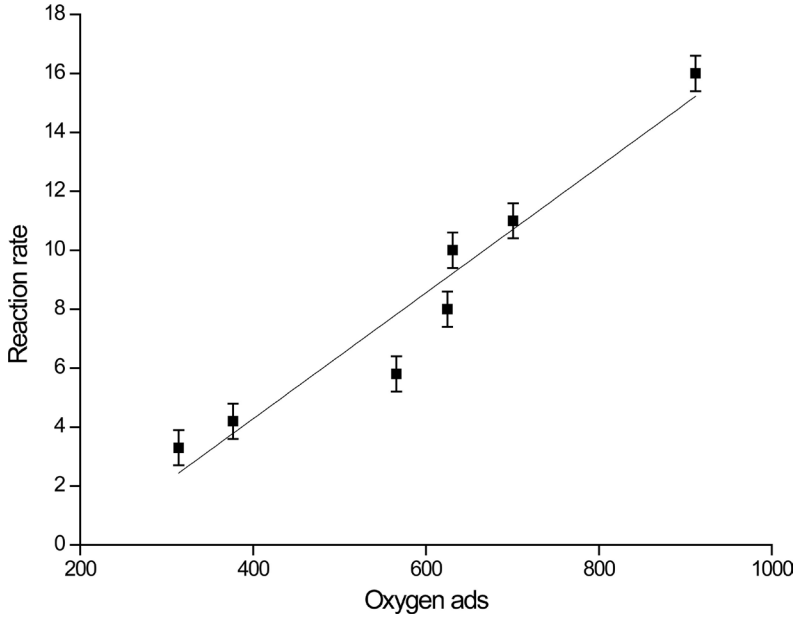

Figure 8. Reaction rate versus the desorbed oxygen.

Table 3. Ignition temperature (T_{50}) and reaction rate at 195˚C.

	T_{50}, ˚C	Reaction rate, μmol·g^{-1}·min^{-1}
$La_{0.6}Ca_{0.4}FeO_3$	275	3.3
$La_{0.6}Ca_{0.4}Fe_{0.9}Ni_{0.1}O_3$	270	4.2
$La_{0.6}Ca_{0.4}Fe_{0.7}Ni_{0.3}O_3$	274	5.8
$La_{0.6}Ca_{0.4}Fe_{0.5}Ni_{0.5}O_3$	243	16
$La_{0.6}Ca_{0.4}Fe_{0.3}Ni_{0.7}O_3$	250	11
$La_{0.6}Ca_{0.4}Fe_{0.1}Ni_{0.9}O_3$	268	10
$La_{0.6}Ca_{0.4}NiO_3$	290	7.6

4. Conclusion

The improvement in the catalytic activity by the progressive substitution in the B-site position of Fe^{3+} by Ni^{2+} in $La_{0.6}Ca_{0.4}Fe_{1-x}Ni_xO_3$ is driven by the formation of oxygen vacancies as well as iron ions in unusual oxidation states (+4). This improvement at lower substitution levels of $x \leq 0.5$ is achieved fundamentally by the oxidation of a portion of the iron ions from Fe^{3+} to Fe^{4+}. At higher Ni doping levels, a large number of oxygen vacancies, segregated phases and a progressive decrease in the perovskite structure are found. The linear dependency of the reaction rate on the oxygen vacancies indicate that the active sites for the DME combustion are directly related to reversible adsorbed oxygen.

Acknowledgements

The authors thank Fondecyt Grants 1130005 and 3150010 and the Red Doctoral REDOC, MINEDUC Project UCo1202.

References

[1] Adamson, A.W. and Gast, A.P. (1997) Physical Chemistry of Surfaces. John Wiley & Sons, Inc., Hoboken.

[2] Li, W.B., Wang, J.X. and Gong, H. (2009) Catalytic Combustion of VOCs on Non-Noble Metal Catalysts. *Catalysis Today*, **148**, 81-87. http://dx.doi.org/10.1016/j.cattod.2009.03.007

[3] Attfield, J.P. (2002) 'A' Cation Control of Perovskite Properties. *Crystal Engineering*, **5**, 427-438. http://dx.doi.org/10.1016/S1463-0184(02)00054-0

[4] Cimino, S., Lisi, L., Pirone, R., Russo, G. and Turco, M. (2000) Methane Combustion on Perovskites-Based Structured Catalysts. *Catalysis Today*, **59**, 19-31. http://dx.doi.org/10.1016/S0920-5861(00)00269-8

[5] Bueno-Lopez, A., Krishna, K., Makkee, M. and Moulijn, J.A. (2005) Enhanced Soot Oxidation by Lattice Oxygen via La^{3+}-Doped CeO_2. *Journal of Catalysis*, **230**, 237-248. http://dx.doi.org/10.1016/j.jcat.2004.11.027

[6] Falcón, H., Barbero, J.A., Alonso, J.A., Martínez-Lope, M.J. and Fierro, J.L.G. (2002) $SrFeO_{3-\delta}$ Perovskite Oxides: Chemical Features and Performance for Methane Combustion. *Chemistry of Materials*, **14**, 2325-2333. http://dx.doi.org/10.1021/cm011292l

[7] Fino, D., Russo, N., Saracco, G. and Speechia, V. (2003) The Role of Suprafacial Oxygen in Some Perovskites for the Catalytic Combustion of Soot. *Journal of Catalysis*, **217**, 367-375. http://dx.doi.org/10.1016/S0021-9517(03)00143-X

[8] Pecchi, G., Jiliberto, M.G., Delgado, E.J., Cadus, L.E. and Fierroc, J.L.G. (2001) Effect of B-Site Cation on the Catalytic Activity of $La_{1-x}CaxBO_3$ (B = Fe, Ni) Perovskite-Type Oxides for Toluene Combustion. *Journal of Chemical Technology and Biotechnology*, **86**, 1067-1073.

[9] Pecchi, G., Reyes, P., Zamora, R., Campos, C., Caduus, L.E. and Barbero, B.P. (2008) Effect of the Preparation Method on the Catalytic Activity of $La_{1-x}Ca_xFeO_3$ Perovskite-Type oxides. *Catalysis Today*, **133-135**, 420-427. http://dx.doi.org/10.1016/j.cattod.2007.11.011

[10] Pecchi, G. and Campos, C. (2007) Structure and Activity of $LaMn_{1-y}Co_yO_3$ Perovskites. *Reaction Kinetics and Catalysis Letters*, **91**, 353-359. http://dx.doi.org/10.1007/s11144-007-5125-1

[11] Lisi, L., Bagnasco, G., Ciambelli, P., De Rossi, S., Porta, P., Russo, G. and Turco, M. (1999) Perovskite-Type Oxides: II. Redox Properties of $LaMn_{1-x}Cu_xO_3$ and $LaCo_{1-x}Cu_xO_3$ and Methane Catalytic Combustion. *Journal of Solid State Chemistry*, **146**, 176-183. http://dx.doi.org/10.1006/jssc.1999.8327

[12] Pecchi, G., Reyes, P., Zamora, R., Cadus, L.E. and Fierro, J.L.G. (2008) Surface Properties and Performance for VOCs Combustion of $LaFe_{1-y}Ni_yO_3$ Perovskite Oxides. *Journal of Solid State Chemistry*, **181**, 905-912. http://dx.doi.org/10.1016/j.jssc.2008.01.020

[13] Bhat, I., Husain, S., Khan, W. and Patil, S.I. (2013) Effect of Zn Doping on Structural, Magnetic and Dielectric Properties of $LaFeO_3$ Synthesized through Sol-Gel Auto-Combustion Process. *Materials Research Bulletin*, **48**, 4506-4512. http://dx.doi.org/10.1016/j.materresbull.2013.07.028

[14] Yu, L., Diao, G.Q., Ye, F., Sun, M., Zhou, J.L., Li, Y.F. and Liu, Y. (2011) Promoting Effect of Ce in Ce/OMS-2 Catalyst for Catalytic Combustion of Dimethyl Ether. *Catalysis Letters*, **141**, 111-119. http://dx.doi.org/10.1007/s10562-010-0475-0

[15] Sun, M., Yu, L., Ye, F., Diao, G.Q., Yu, Q., Hao, Z.F., Zheng, Y.Y. and Yuan, L.X. (2013) Transition Metal Doped Cryptomelane-Type Manganese Oxide for Low-Temperature Catalytic Combustion of Dimethyl Ether. *Chemical Engineering Journal*, **220**, 320-327. http://dx.doi.org/10.1016/j.cej.2013.01.061

[16] Zhou, J.L., Yu, L., Sun, M., Diao, G.Q., Li, Y.F. and Cheng, X.L. (2013) Enhanced Activity and Stability of Al_2O_3-

Pillared Layered Manganese Oxides for DME Combustion. *Microporous and Mesoporous Materials*, **181**, 105-110. http://dx.doi.org/10.1016/j.micromeso.2013.07.023

[17] Porta, P., De Rossi, S., Faticanti, M., Minelli, G., Pettiti, I., Lisi, L. and Turco, M. (1999) Perovskite-Type Oxides: I. Structural, Magnetic, and Morphological Properties of $LaMn_{1-x}Cu_xO_3$ and $LaCo_{1-x}Cu_xO_3$ Solid Solutions with Large Surface Area. *Journal of Solid State Chemistry*, **146**, 291-304. http://dx.doi.org/10.1006/jssc.1999.8326

[18] Ciambelli, P., Cimino, S., Lisi, L., Faticanti, M., Minelli, G., Pettiti, I. and Porta, P. (2001) La, Ca and Fe Oxide Perovskites: Preparation, Characterization and Catalytic Properties for Methane Combustion. *Applied Catalysis B*: *Environmental*, **33**, 193-203. http://dx.doi.org/10.1016/S0926-3373(01)00163-1

[19] Russo, N., Fino, D., Saracco, G. and Specchia, V. (2005) Studies on the Redox Properties of Chromite Perovskite Catalysts for Soot Combustion. *Journal of Catalysis*, **229**, 459-469. http://dx.doi.org/10.1016/j.jcat.2004.11.025

[20] Merino, N.A., Barbero, B.P., Grange, P. and Cadús, L.E. (2005) $La_{1-x}Ca_xCoO_3$ Perovskite-Type Oxides: Preparation, Characterisation, Stability, and Catalytic Potentiality for the Total Oxidation of Propane. *Journal of Catalysis*, **231**, 232-244. http://dx.doi.org/10.1016/j.jcat.2005.01.003

[21] Buciuman, F.C., Patcas, F. and Zsakó, J. (2000) TPR-Study of Substitution Effects on Reducibility and Oxidative Non-Stoichiometry of $La_{0.8}A'_{0.2}MnO_{3+\delta}$ Perovskites. *Journal of Thermal Analysis and Calorimetry*, **61**, 819-825. http://dx.doi.org/10.1023/A:1010153331841

[22] Tejuca, L.G., Fierro, J.L.G. and Tascon, J.M.D. (1989) Structure and Reactivity of Perovskite-Type Oxides. *Advances in Catalysis*, **36**, 237-328. http://dx.doi.org/10.1016/S0360-0564(08)60019-X

[23] Lee, Y.N., Lago, R.M., Fierro, J.L.G., Cortes, V., Sapina, F. and Martinez, E. (2001) Surface Properties and Catalytic Performance for Ethane Combustion of $La_{1-x}K_xMnO_{3+\delta}$ Perovskites. *Applied Catalysis A*: *General*, **207**, 17-24. http://dx.doi.org/10.1016/S0926-860X(00)00610-4

[24] Fu, M.L., Yue, X.H., Ye, D.Q., Ouyang, J.H., Huang, B.C., Wu, J.H. and Liang, H. (2010) Soot Oxidation via CuO Doped CeO_2 Catalysts Prepared Using Coprecipitation and Citrate Acid Complex-Combustion Synthesis. *Catalysis Today*, **153**, 125-132. http://dx.doi.org/10.1016/j.cattod.2010.03.017

[25] Taguchi, H., Sugita, A., Nagao, M. and Tabata, K. (1995) Surface Characterization of $LaMnO_{3+\delta}$ Powder Annealed in Air. *Journal of Solid State Chemistry*, **119**, 164-168. http://dx.doi.org/10.1016/0022-4596(95)80025-K

[26] Reyes, P., Pecchi, G. and Fierro, J.L.G. (2001) Surface Structures of Rh-Cu Sol-Gel Catalysts and Performance for Crotonaldehyde Hydrogenation. *Langmuir*, **17**, 522-527. http://dx.doi.org/10.1021/la0006418

[27] Aneggi, E., Llorca, J., de Leitenburg, C., Dolcetti, G. and Trovarelli, A. (2009) Soot Combustion Over Silver-Supported Catalysts. *Applied Catalysis B*: *Environmental*, **91**, 489-498. http://dx.doi.org/10.1016/j.apcatb.2009.06.019

[28] Dhakad, M., Mitshuhashi, T., Rayalu, S., Doggali, P., Bakardjiva, S., Subrt, J., Fino, D., Haneda, H. and Labhsetwar, N. (2008) Co_3O_4-CeO_2 Mixed Oxide-Based Catalytic Materials for Diesel Soot Oxidation. *Catalysis Today*, **132**, 188-193. http://dx.doi.org/10.1016/j.cattod.2007.12.035

[29] Ciambelli, P., Cimino, S., De Rossi, S., Faticanti, M., Lisi, L., Minelli, G., Pettiti, I., Porta, P., Russo, G. and Turco, M. (2000) $AMnO_3$ (A=La, Nd, Sm) and $Sm_{1-x}Sr_xMnO_3$ Perovskites as Combustion Catalysts: Structural, Redox and Catalytic Properties. *Applied Catalysis B*: *Environmental*, **24**, 243-253. http://dx.doi.org/10.1016/S0926-3373(99)00110-1

[30] Bialobok, B., Trawczynski, J., Mista, W. and Zawadzki, M. (2007) Ethanol Combustion Over Strontium- and Cerium-Doped $LaCoO_3$ Catalysts. *Applied Catalysis B*: *Environmental*, **72**, 395-403. http://dx.doi.org/10.1016/j.apcatb.2006.12.006

[31] Pereniguez, R., Hueso, J.L., Gaillard, F., Holgado, J.P. and Caballero, A. (2012) Study of Oxygen Reactivity in $La_{1-x}Sr_xCoO_{3-\delta}$ Perovskites for Total Oxidation of Toluene. *Catalysis Letters*, **142**, 408-416. http://dx.doi.org/10.1007/s10562-012-0799-z

[32] Zhang, J.Y., Tan, D.D., Meng, Q.J., Weng, X.L. and Wu, Z.B. (2015) Structural Modification of $LaCoO_3$ Perovskite for Oxidation Reactions: The Synergistic Effect of Ca^{2+} and Mg^{2+} Co-Substitution on Phase Formation and Catalytic Performance. *Applied Catalysis B*: *Environmental*, **172**, 18-26. http://dx.doi.org/10.1016/j.apcatb.2015.02.006

[33] Jimenez, R., Zamora, R., Pecchi, G., Garcia, X. and Gordon, A.L. (2010) Effect of Ca-Substitution in $La_{1-x}Ca_xFeO_3$ Perovskites on the Catalytic Activity for Soot Combustion. *Fuel Processing Technology*, **91**, 546-549. http://dx.doi.org/10.1016/j.fuproc.2009.12.017

[34] Seyfi, B., Baghalha, M. and Kazemian, H. (2009) Modified $LaCoO_3$ Nano-Perovskite Catalysts for the Environmental Application of Automotive CO Oxidation. *Chemical Engineering Journal*, **148**, 306-311. http://dx.doi.org/10.1016/j.cej.2008.08.041

[35] Ivanov, D.V., Pinaeva, L.G., Sadovskaya, E.M. and Isupova, L.A. (2011) Influence of the Mobility of Oxygen on the Reactivity of $La_{1-x}Sr_xMnO_3$ Perovskites in Methane Oxidation. *Kinetics and Catalysis*, **52**, 401-408. http://dx.doi.org/10.1134/S0023158411030086